



LUND UNIVERSITY

Cramér-Rao lower bounds for inverse scattering problems of multilayer structures

Gustafsson, Mats; Nordebo, Sven

2006

[Link to publication](#)

Citation for published version (APA):

Gustafsson, M., & Nordebo, S. (2006). *Cramér-Rao lower bounds for inverse scattering problems of multilayer structures*. (Technical Report LUTEDX/(TEAT-7148)/1-23/(2006); Vol. TEAT-7148). [Publisher information missing].

Total number of authors:

2

General rights

Unless other specific re-use rights are stated the following general rights apply:

Copyright and moral rights for the publications made accessible in the public portal are retained by the authors and/or other copyright owners and it is a condition of accessing publications that users recognise and abide by the legal requirements associated with these rights.

- Users may download and print one copy of any publication from the public portal for the purpose of private study or research.
- You may not further distribute the material or use it for any profit-making activity or commercial gain
- You may freely distribute the URL identifying the publication in the public portal

Read more about Creative commons licenses: <https://creativecommons.org/licenses/>

Take down policy

If you believe that this document breaches copyright please contact us providing details, and we will remove access to the work immediately and investigate your claim.

LUND UNIVERSITY

PO Box 117
221 00 Lund
+46 46-222 00 00

Cramér-Rao lower bounds for inverse scattering problems of multilayer structures

Mats Gustafsson and Sven Nordebo

Department of Electrosience
Electromagnetic Theory
Lund Institute of Technology
Sweden



Mats Gustafsson

Department of Electrosience
Electromagnetic Theory
Lund Institute of Technology
P.O. Box 118
SE-221 00 Lund
Sweden

Sven Nordebo

School of Mathematics and System Engineering
Växjö University
Växjö
Sweden

Editor: Gerhard Kristensson

© Mats Gustafsson and Sven Nordebo, Lund, August 30, 2006

Abstract

In this paper, the inverse scattering problem of a multilayer structure is analyzed with the Fisher information matrix and the Cramér-Rao lower bound. The Cramér-Rao lower bound quantifies the ill-posedness of the inverse scattering problem in terms of resolution contra estimation accuracy based on the observation of noisy data. The limit for feasible inversion is identified by an asymptotic eigenvalue analysis of the Toeplitz Fisher information matrix and an application of the sampling theorem. It is shown that the resolution is inversely proportional to the bandwidth of the reflection data and that the Cramér-Rao lower bound increases linearly with the number of slabs. The transmission data gives a rank one Fisher information matrix which can approximately reduce the Cramér-Rao lower bound a factor of four. Moreover, the effect of dispersive material parameters and simultaneous estimation of two material parameters are analyzed. The results are illustrated with numerical examples.

1 Introduction

Inverse scattering problems are in general ill-posed, *i.e.*, they are not well-posed in the sense of existence, uniqueness, and continuous dependence of the solution on the data [10, 13]. The uniqueness theorems typically show that the solution is unique if data is available from all possible measurements. This is very important but not sufficient from a practical point of view. Further, since the solution of ill-posed problems does not depend continuously on the data, the effect of noise on the solution is amplified in a way that calls for proper control. For this purpose, a sensitivity analysis based on *regularization theory* [1] is often used to control the imaging error. The number of degrees of freedom that pertains the number of significant singular values of a linear operator is a very useful tool in linear inverse scattering problems, see *e.g.*, [1, 3, 21]. The number of degrees of freedom, which is virtually independent of the noise level, can be used to estimate the number of retrievable parameters of an object, and hence the resolution. However, these approaches are rather coarse and do not give a qualitative measure on the information content of the inversion data with respect to the accuracy and the resolution of images.

Estimation theory is a classical and well developed area within signal processing research and mathematical statistics. Over several decades the Cramér-Rao lower bound has been subjected to many revivals and has become the dominating tool in areas such as statistical signal processing [12], array signal processing [14] and systems and control theory [22]. There is obviously many connections between inverse scattering and estimation [17, 18, 23]. The Cramér-Rao lower bound is a quantitative measure that give us the best possible measurement performance associated with *any* unbiased estimation, a performance which is *achievable* with linear models, and *asymptotically achievable* under very general conditions [12].

In inverse scattering problems of a multilayer slab the fields are observed at one side of the object or at both sides, *i.e.*, one uses reflection and (or) transmission data. The one-dimensional case have been thoroughly studied in both the time- and

frequency-domains [2, 15]. The one-dimensional inverse scattering problem of an inhomogeneous slab is preferably solved in the time-domain with wave splitting [2, 4, 15, 16] or least-squares optimization [8, 24]. The wave splitting algorithms are restricted to identification of the permittivity or simultaneous identification of the permittivity and conductivity [15, 16].

In this paper, the inverse scattering problem of a multilayer structure is analyzed with the Fisher information matrix (FIM) and the Cramér-Rao lower bound (CRLB). The Cramér-Rao lower bound quantifies the ill-posedness of the inverse scattering problem in terms of resolution contra estimation accuracy based on the observation of noisy data. The limit for feasible inversion is identified by an asymptotic eigenvalue analysis of the Toeplitz Fisher information matrix and an application of the sampling theorem. It is shown that the resolution is inversely proportional to the bandwidth of the reflection data and that the Cramér-Rao lower bound increases linearly with the number of slabs. The transmission data gives a rank one Fisher information matrix which can reduce the Cramér-Rao lower bound approximately a factor of four. Moreover, the effect of dispersive material parameters and simultaneous estimation of two material parameters are analyzed. The results are illustrated with numerical examples.

It should be noted that the time domain Gaussian signal model described in this paper is used mainly to gain fundamental physical insight about the inverse problem at hand. In a practical situation, it may also be important to consider proper noise filtering using short time windowing of data.

The paper is organized as follows. We review the Fisher information matrix and the Cramér-Rao lower bound in Section 2. The Fisher information matrices of reflection and transmission data are analyzed in Sections 3 and 4, respectively. The effect of the Cramér-Rao lower bound in a lossy background is discussed in Section 6. Estimation of dispersive material parameters are considered in Section 7. Conclusions and a discussion are given in Section 8.

2 Fisher information of multilayer structures

We use the Fisher information and the Cramér-Rao lower bound to analyze the information content in different measurement situations of multilayer structures. The transmitted and reflected fields can be observed in the inverse scattering problem. It is possible to observe the fields for different spectral contents, incident angles, and polarizations. We consider N_{ob} separate time-domain measurements of either the reflected or transmitted field with arbitrary incident angles and polarizations. This gives the time-domain measurement model

$$\mathbf{x}(t) = \boldsymbol{\mu}(\boldsymbol{\xi}, t) + \mathbf{n}(t) \quad (2.1)$$

where $\mathbf{x}(t)$ is the measurement vector, $\boldsymbol{\mu}(\boldsymbol{\xi}, t)$ the physically based signal model, $\boldsymbol{\xi}$ the parameter vector, and $\mathbf{n}(t)$ the noise. It is assumed that $\mathbf{n}(t)$ is a wide sense stationary complex Gaussian random process with correlation function

$$\mathbf{R}(\tau) = \mathcal{E}\{\mathbf{n}(t + \tau)\mathbf{n}^H(t)\}. \quad (2.2)$$

Moreover, it is assumed that the different measurements are uncorrelated giving a diagonal correlation matrix, $[\mathbf{R}(\tau)]_{ij} = R_j(\tau)\delta_{ij}$, where $[\]_{ij}$ denotes the element in row i and column j .

Consider the finite time interval $-T/2 \leq t \leq T/2$ and let $\tilde{\mathbf{x}}(k)$ denote the Fourier series representation of the signal $\mathbf{x}(t)$

$$\tilde{\mathbf{x}}(\kappa) = \frac{1}{T} \int_{-T/2}^{T/2} \mathbf{x}(t) e^{-i\kappa \frac{2\pi}{T} t} dt, \quad \kappa \in \mathbb{Z}. \quad (2.3)$$

The Fourier series of $\boldsymbol{\mu}$ is similarly denoted $\tilde{\boldsymbol{\mu}}$. Let τ_w denote the time-domain support of the autocorrelation function $\mathbf{R}(\tau)$. It is then easy to show that if $T \gg \tau_w$ then

$$\mathbf{C}_{\kappa l} = \mathcal{E} \left\{ (\tilde{\mathbf{x}}(\kappa) - \tilde{\boldsymbol{\mu}}(\kappa)) (\tilde{\mathbf{x}}(l) - \tilde{\boldsymbol{\mu}}(l))^H \right\} = \frac{1}{T} \mathbf{P} \left(\kappa \frac{2\pi}{T} \right) \delta_{\kappa l}, \quad (2.4)$$

where \mathbf{P} is a diagonal matrix, $[\mathbf{P}]_{ij} = P_j \delta_{ij}$, given by the Fourier transform of $\mathbf{R}(\tau)$, *i.e.*, the *spectral density* $P_j(\omega)$ of measurement j is the Fourier transform of the corresponding autocorrelation $R_j(\tau)$.

Now, the Fisher information matrix [12] is given by

$$\begin{aligned} [\mathcal{I}(\boldsymbol{\xi})]_{mn} &= \sum_{\kappa=-\infty}^{\infty} 2 \operatorname{Re} \left\{ \frac{\partial \tilde{\boldsymbol{\mu}}^H(\kappa)}{\partial \xi_m} \mathbf{C}_{\kappa\kappa}^{-1} \frac{\partial \tilde{\boldsymbol{\mu}}(\kappa)}{\partial \xi_n} \right\} \\ &= \frac{1}{2\pi} \sum_{j=1}^{N_{\text{ob}}} \sum_{\kappa=-\infty}^{\infty} \frac{2}{P_j(\kappa \frac{2\pi}{T})} \operatorname{Re} \left\{ \frac{\partial T \tilde{\mu}_j^*(\kappa)}{\partial \xi_m} \frac{\partial T \tilde{\mu}_j(\kappa)}{\partial \xi_n} \right\} \frac{2\pi}{T}. \end{aligned} \quad (2.5)$$

Since the Fourier transform of $\boldsymbol{\mu}(t)$ is given by

$$\hat{\boldsymbol{\mu}}(\omega) = \int_{-\infty}^{\infty} \boldsymbol{\mu}(t) e^{-i\omega t} dt \quad (2.6)$$

and $T \tilde{\boldsymbol{\mu}}(k) \rightarrow \hat{\boldsymbol{\mu}}(\omega)$ as $T \rightarrow \infty$, the Fisher information matrix in (2.5) becomes

$$[\mathcal{I}(\boldsymbol{\xi})]_{mn} = \sum_{j=1}^{N_{\text{ob}}} \frac{1}{2\pi} \int_{-\infty}^{\infty} \frac{2}{P_j(\omega)} \operatorname{Re} \left\{ \frac{\partial \hat{\mu}_j^*(\omega)}{\partial \xi_m} \frac{\partial \hat{\mu}_j(\omega)}{\partial \xi_n} \right\} d\omega. \quad (2.7)$$

The Cramer-Rao lower bound (CRLB) is a quantitative measure that gives the best possible measurement performance associated with *any* unbiased estimation, a performance which is *achievable* with linear models, and *asymptotically achievable* under very general conditions [12]. The Cramér-Rao lower bound for estimating the parameter ξ_n is given by

$$\operatorname{var}\{\xi_n\} \geq [\mathcal{I}^{-1}(\boldsymbol{\xi})]_{nn}. \quad (2.8)$$

We consider a layered medium consisting of N homogeneous, isotropic and non-magnetic dielectric slabs with thickness d , see Figure 1. The impedance of slab number n is $\eta_n = \sqrt{\mu_0/\epsilon_n}$ and the impedance of the surrounding medium is $\eta_0 = \sqrt{\mu_0/\epsilon_0}$,

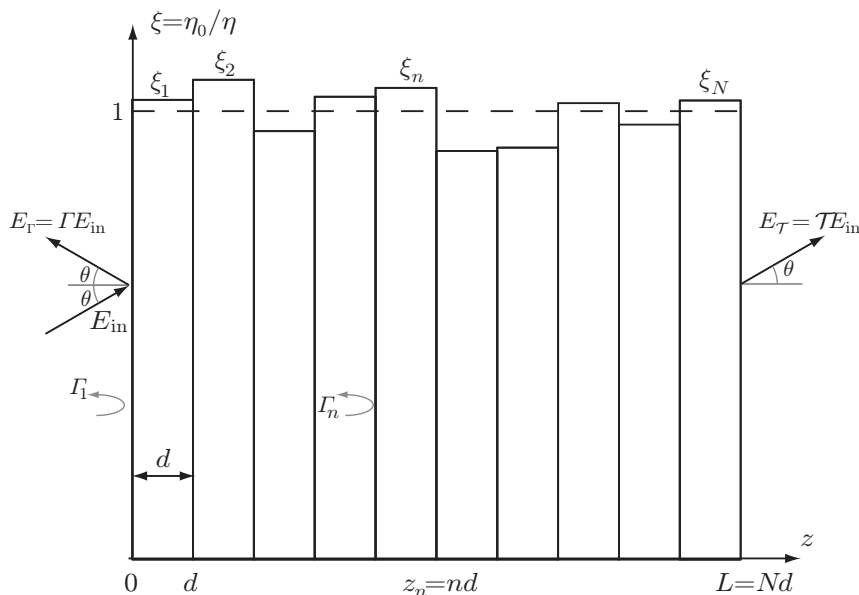


Figure 1: Illustration of the multilayer structure consisting of N dielectric slabs with impedance $\eta_n = \eta_0/\xi_n$. A plane wave, E_{in} , impinging at the incident angle θ produces a reflected wave E_{Γ} and the transmitted wave $E_{\mathcal{T}}$.

where ϵ and μ denote the permittivity and permeability, respectively. The relative admittance of the slabs is denoted $\boldsymbol{\xi} = (\xi_1, \xi_2, \dots, \xi_N)$, where $\xi_n = \eta_0/\eta_n$. The relative admittance of the slab is greater (smaller) than 1 if the medium is denser (thinner) than the background. We use a Fourier representation of the electromagnetic fields where a plane wave, \mathbf{E}_{in} , impinges on the structure with incident angle θ . The reflected wave, \mathbf{E}_{Γ} , is given by the reflection coefficient, Γ , *i.e.*, $\mathbf{E}_{\Gamma} = \Gamma \mathbf{E}_{\text{in}}$. The transmitted wave, $\mathbf{E}_{\mathcal{T}}$, is similarly given by the transmission coefficient, \mathcal{T} , *i.e.*, $\mathbf{E}_{\mathcal{T}} = \mathcal{T} \mathbf{E}_{\text{in}}$. We assume that the illuminating wave field, \mathbf{E}_{in} , has spectral support in the frequency range $\omega_1 \leq \omega \leq \omega_2$. Moreover, we also assume that the quotient between the spectral densities of the illuminating wave field and the noise is frequency independent.

It is convenient to normalize the measured data with the amplitude of the illuminating wave and at the same time introduce the dimensionless parameter

$$\sigma_j^2 = \frac{\pi P_j}{|\mathbf{E}_{\text{in}}|^2 \Delta\omega} \quad (2.9)$$

to quantify the noise level, where $\Delta\omega = \omega_2 - \omega_1$ denotes the bandwidth. This simplifies the FIM to

$$[\mathcal{I}(\boldsymbol{\xi})]_{mn} = \sum_{j=1}^{N_{\text{ob}}} \frac{2}{\sigma_j^2 \Delta\omega} \text{Re} \int_{\omega_1}^{\omega_2} \left(\frac{\partial \hat{\mu}_j}{\partial \xi_m} \right)^* \frac{\partial \hat{\mu}_j}{\partial \xi_n} d\omega = \sum_{j=1}^{N_{\text{ob}}} \mathcal{I}^{(j)}(\boldsymbol{\xi}), \quad (2.10)$$

where $\hat{\mu}_j$ is the reflection or transmission coefficient and $|\mathbf{E}_{\text{in}}|$ is normalized to unity. We also observe that the FIM can be written as the sum of the FIM corresponding

to each observation. In particular, we can consider observations of the reflection coefficient and transmission coefficient separately.

3 FIM of the reflection coefficient

For observations of the reflection coefficient, we use a recursive relation between the reflection coefficients Γ_n , $n = 1, \dots, N$, in the multilayer structure, see Figure 1. The reflection coefficients, Γ_n , in the multilayer structure is determined by the reflection coefficient Γ_{n+1} as [20]

$$\Gamma_n = \frac{\rho_n + \Gamma_{n+1}e^{-2ik_{z,n}d}}{1 + \rho_n\Gamma_{n+1}e^{-2ik_{z,n}d}}, \quad (3.1)$$

where $k_{z,n} = k\xi_n \cos \theta_n$ is the z -component of the wave number, k , and ρ_n is the elementary reflection coefficient given by

$$\rho_n = \frac{\eta_{T,n} - \eta_{T,n-1}}{\eta_{T,n} + \eta_{T,n-1}}, \quad (3.2)$$

where the transverse impedance $\eta_{T,n}$ is

$$\eta_{TE,n} = \frac{\eta_n}{\cos \theta_n} \quad \text{and} \quad \eta_{TM,n} = \eta_n \cos \theta_n, \quad (3.3)$$

in the TE and TM polarizations, respectively.

The FIM of the reflection coefficient is determined by the derivatives of the reflection coefficient with respect to the parameters ξ_n . We evaluate the FIM at the background admittance $\boldsymbol{\xi} = \mathbf{1}$ to simplify the expressions. This gives

$$\begin{aligned} \left. \frac{\partial \Gamma_n}{\partial \xi_n} \right|_{\boldsymbol{\xi}=\mathbf{1}} &= \left. \frac{\partial \Gamma_n}{\partial \rho_n} \frac{\partial \rho_n}{\partial \xi_n} \right|_{\boldsymbol{\xi}=\mathbf{1}} + \left. \frac{\partial \Gamma_n}{\partial \Gamma_{n+1}} \frac{\partial \Gamma_{n+1}}{\partial \rho_{n+1}} \frac{\partial \rho_{n+1}}{\partial \xi_n} \right|_{\boldsymbol{\xi}=\mathbf{1}} + \left. \frac{\partial \Gamma_n}{\partial k_{z,n}} \frac{\partial k_{z,n}}{\partial \xi_n} \right|_{\boldsymbol{\xi}=\mathbf{1}} \\ &= \left. \frac{\partial \rho_n}{\partial \xi_n} \right|_{\boldsymbol{\xi}=\mathbf{1}} + e^{-2ikd \cos \theta} \left. \frac{\partial \rho_{n+1}}{\partial \xi_n} \right|_{\boldsymbol{\xi}=\mathbf{1}} = (1 - e^{-2ikd \cos \theta}) \left. \frac{\partial \rho_n}{\partial \xi_n} \right|_{\boldsymbol{\xi}=\mathbf{1}}, \end{aligned} \quad (3.4)$$

where the derivatives of the elementary reflection coefficients are

$$\frac{\partial \rho_n}{\partial \xi_n} = \frac{\partial \rho_n}{\partial \eta_{T,n}} \frac{\partial \eta_{T,n}}{\partial \xi_n} = \frac{1}{2\eta_T} \frac{\partial \eta_{T,n}}{\partial \xi_n} \quad \text{and} \quad \frac{\partial \rho_{n+1}}{\partial \xi_n} = -\frac{\partial \rho_n}{\partial \xi_n} \quad (3.5)$$

for $\boldsymbol{\xi} = \mathbf{1}$. The derivative of the transverse impedance is determined with the Snell's law $\xi_n \sin \theta_n = \xi_{n-1} \sin \theta_{n-1}$ that gives $\cos \theta_n = \sqrt{\xi_n^2 - \xi_{n-1}^2 \sin^2 \theta_{n-1}} / \xi_n$ and hence

$$\left. \frac{\partial \rho_n}{\partial \xi_n} \right|_{\boldsymbol{\xi}=\mathbf{1}} = \begin{cases} \frac{1}{2 \cos \theta} \frac{\partial}{\partial \xi_n} \frac{\sqrt{\xi_n^2 - \sin^2 \theta}}{\xi_n^2} = \frac{\sin^2 \theta - \cos^2 \theta}{2 \cos^2 \theta} = -\frac{1 - \tan^2 \theta}{2}, & \text{(TM)} \\ \frac{\cos \theta}{2} \frac{\partial}{\partial \xi_n} \frac{1}{\sqrt{\xi_n^2 - \sin^2 \theta}} = \frac{-1}{2 \cos^2 \theta} = -\frac{1 + \tan^2 \theta}{2}, & \text{(TE)} \end{cases} \quad (3.6)$$

in the TM and TE polarizations, respectively. The derivative of the reflection coefficient at the first interface is finally related to the derivative of the reflection coefficient of interface number n with a phase shift, giving

$$\left. \frac{\partial \Gamma_1}{\partial \xi_n} \right|_{\boldsymbol{\xi}=\mathbf{1}} = -e^{-2i(n-1)kd \cos \theta} \frac{1 - e^{-2ikd \cos \theta}}{2} (1 \pm \tan^2 \theta), \quad (3.7)$$

where the + and – signs correspond to the TE and TM cases, respectively. Observe that the polarization only enters the derivative with the $1 \pm \tan^2 \theta$ term. The derivative increases (decreases) with increasing angle for the TE (TM) case. This can be understood as the interaction between the dielectric slab and the electromagnetic field is dominated by the electric part of the field. We also observe that the derivative is zero in the TM case for $\theta = \pi/4$.

The FIM of the reflection coefficient evaluated at $\boldsymbol{\xi} = \mathbf{1}$ has the elements

$$\begin{aligned} [\mathcal{I}_\Gamma]_{mn} &= \frac{2}{\sigma_\Gamma^2 \Delta\omega} \operatorname{Re} \int_{\omega_1}^{\omega_2} \frac{\partial \Gamma}{\partial \xi_m} \left(\frac{\partial \Gamma}{\partial \xi_n} \right)^* d\omega \\ &= \frac{2}{\sigma_\Gamma^2 \Delta k} \operatorname{Re} \int_{k_1}^{k_2} e^{2ikd(n-m)\cos\theta} \frac{|1 - e^{-2ikd\cos\theta}|^2}{4} dk (1 \pm \tan^2 \theta)^2, \end{aligned} \quad (3.8)$$

where the wave numbers $k_i = \omega_i/c_0$, $i = 1, 2$ and bandwidth $\Delta k = \Delta\omega/c_0$ are used. This gives the FIM

$$\begin{aligned} [\mathcal{I}_\Gamma]_{mn} &= \frac{1}{2\tilde{\sigma}_\Gamma^2 \Delta k} \operatorname{Re} \int_{k_1}^{k_2} 2e^{2ikd(n-m)\cos\theta} - e^{2ikd(n-m-1)\cos\theta} - e^{2ikd(n-m+1)\cos\theta} dk \\ &= \frac{1}{2\tilde{\sigma}_\Gamma^2} (2f_{n-m} - f_{n-m-1} - f_{n-m+1}), \end{aligned} \quad (3.9)$$

where

$$f_n = \cos(2k_c dn \cos\theta) \frac{\sin(\Delta k dn \cos\theta)}{\Delta k dn \cos\theta} = \frac{\sin(2k_2 dn \cos\theta) - \sin(2k_1 dn \cos\theta)}{2\Delta k dn \cos\theta}, \quad (3.10)$$

and the scaled noise level $\tilde{\sigma}_\Gamma^2 = \sigma_\Gamma^2/(1 \pm \tan^2 \theta)^2$ and the center wave number $k_c = \omega_c/c_0 = (k_1 + k_2)/2$ are introduced to simplify the notation. We observe that the diagonal elements of the FIM are identical, *i.e.*, the sensitivity of the parameters are the same. The FIM is an $N \times N$ Toeplitz matrix or convolution matrix, see Appendix A. Before we analyze the general FIM we consider the special but important case

$$\Delta k d \cos\theta = \pi \quad (3.11)$$

giving $f_p = \delta_{p,0}$ and hence a FIM in the form of the simple bidiagonal Toeplitz matrix

$$\mathcal{I}_\Gamma = \frac{1}{2\tilde{\sigma}_\Gamma^2} \begin{pmatrix} 2 & -1 & 0 & \dots & 0 \\ -1 & 2 & -1 & \dots & 0 \\ 0 & -1 & 2 & \dots & 0 \\ \vdots & \vdots & \vdots & \ddots & \vdots \\ 0 & 0 & 0 & \dots & 2 \end{pmatrix} = \frac{1}{2\tilde{\sigma}_\Gamma^2} \mathbf{T}_1. \quad (3.12)$$

The inverse of this matrix is well defined, see Appendix A, with the diagonal elements giving the CRLB

$$[\mathcal{I}_\Gamma^{-1}]_{nn} = 2\tilde{\sigma}_\Gamma^2 \frac{n(N+1-n)}{N+1} \leq \tilde{\sigma}_\Gamma^2 \frac{N+1}{2}. \quad (3.13)$$

The CRLB reaches its maximal value, $\tilde{\sigma}_\Gamma^2(N+1)/2$, for odd N in the center of the structure, $n = (N+1)/2$, and its smallest value, $2\tilde{\sigma}_\Gamma^2 N/(N+1)$, at the edges of the structure, $n = 1$ and $n = N$. We observe that the CRLB grows linearly with N in the center of the structure and is independent of N at the edges of the structure.

The general Toeplitz matrix corresponding to the FIM (3.9) is analyzed in Appendix A, where it is shown that the CRLB can be decomposed into two regions depending on the product between the bandwidth, Δk , and the resolution, d , *i.e.*,

$$\begin{cases} \Delta k d \cos \theta < \gamma \pi \Rightarrow [\mathcal{I}_\Gamma^{-1}]_{nn} \sim \tilde{\sigma}_\Gamma^2 \beta_n^N \text{ for some } \beta_n > 1 \\ \Delta k d \cos \theta > \gamma \pi \Rightarrow [\mathcal{I}_\Gamma^{-1}]_{nn} \approx 2\tilde{\sigma}_\Gamma^2 \frac{n(N+1-n)}{N+1} \end{cases} \quad (3.14)$$

where γ is a number $1/2 \leq \gamma \leq 1$ that can be determined as

$$\gamma = 1 - \min_{m \in \mathbb{Z}} (|2k_c d / \pi - m|). \quad (3.15)$$

The Cramér-Rao lower bound is increasing very fast with N in the first region where $\Delta k d \cos \theta < \gamma \pi$ and hence it is not realistic to resolve these fine structures as it would require an extremely good signal-to-noise ratio if the number of slabs is large. This is an illustration of the ill-posedness of the inverse scattering problem, *i.e.*, very small errors in the data can give very large errors in the estimated parameters. The situation changes as $\Delta k d \cos \theta$ increases and for $\Delta k d \cos \theta \geq \gamma \pi$ the problem is basically well posed. The CRLB shows that the errors of an optimal estimator only increases linearly with the number of slabs. To conclude, the resolution, d , is inversely proportional to the absolute bandwidth Δk or equivalently expressed in the fractional bandwidth, $B = \Delta k / k_c$, and the center wavelength, λ_c , as

$$B \frac{d}{\lambda_c} \geq \frac{\gamma}{2}. \quad (3.16)$$

The corresponding CRLB in the resolved region is proportional to N .

It is illustrative to use the highest wavenumber k_2 or equivalently the shortest wavelength, $\lambda_2 = 2\pi/k_2$ to quantify the resolution for a broadband signal. The special cases

$$2k_2 d \cos \theta = m\pi \quad \text{and} \quad 2k_1 d \cos \theta = (m-1)\pi \quad (3.17)$$

with $m = 1, 2, \dots$ in (3.10), give a bidiagonal Toeplitz matrix of the form (3.12). This is an example of the resolution limit $\Delta k d \cos \theta = \pi/2$, *i.e.*, $\gamma = 1/2$, or expressed in λ_2

$$d \geq \gamma \lambda_2 \frac{1 + B/2}{2B \cos \theta} \geq \frac{\gamma \lambda_2}{2 \cos \theta}. \quad (3.18)$$

We also observe that (3.17) with $m = 1$ gives a quarter of a wavelength resolution for $\theta = 0$.

The maximal value of the Cramér-Rao bound with $\sigma_\Gamma^2(N+1) = 2$ and $\theta = 0$ is shown in Figure 2a as a function of the relative bandwidth B for the different resolutions $d/\lambda_2 = m/4$, $m = 1, 2, 3, 5, 7$ and number of slabs $N = 100, 150, 200$. We observe that the CRLB is very large for bandwidths under the $\gamma = 1/2$ limit as

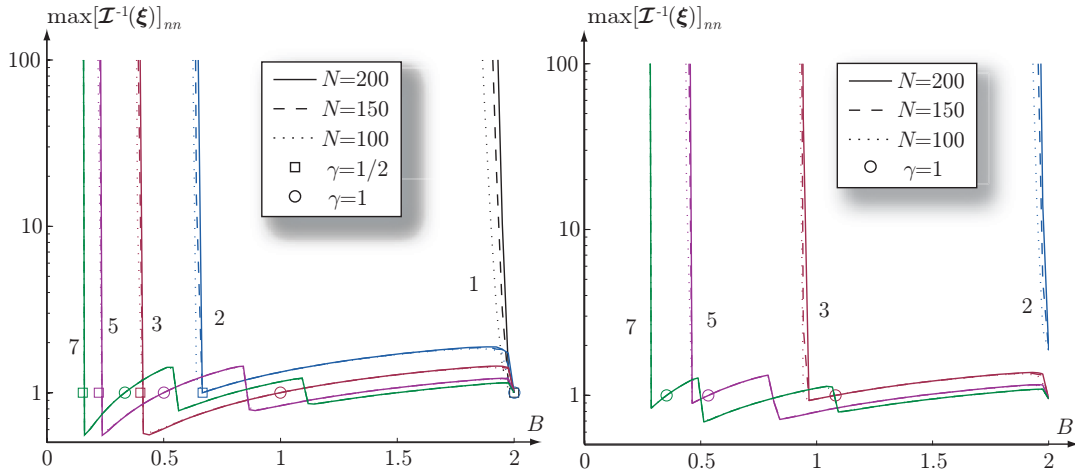


Figure 2: Cramér-Rao lower bound at the center of the structure, $n = N/2$, for $\sigma_{\Gamma}^2(N+1) = 2$ and $\theta = 0$ as a function of the relative bandwidth B . a) the resolution $d/\lambda_2 = m/4$, $m = 1, 2, 3, 5, 7$. b) the resolutions $d/\lambda_2 = 0.95m/4$, $m = 1, 2, 3, 5, 7$.

indicated by the square symbols. Here, it is also seen that the quarter wavelength resolution $d = \lambda_2/4$ requires $B = 2$ is seen in (3.18). The combination (3.17) gives the highest resolution for a given bandwidth, *i.e.*, (3.18) with $\gamma = 1/2$. The situation is drastically changed as the resolution is reduced under the optimal choice (3.17) as seen in Figure 2b, where the resolution $\lambda_2/d = 0.95m/4$ is considered. It is seen that the bandwidth is close to the one corresponding to (3.14) with $\gamma = 1$ as indicated by the circles in the figure. The small oscillations in the CRLB depend on the scaling of the noise with the bandwidth. The amount of Fisher information of a set of observations is in general increasing if the set of observations increases, *e.g.*, a larger bandwidth should be better for the same upper frequency. However, as we assumed a noise level proportional to the bandwidth, *i.e.*, $P_j \sim \sigma^2 \Delta\omega$ in (3.9), we have to scale the FIM with the relative bandwidth, *i.e.*,

$$B_1 \mathcal{I}_{\Gamma}(B = B_1) \leq B_2 \mathcal{I}_{\Gamma}(B = B_2) \quad \text{if } B_1 \leq B_2. \quad (3.19)$$

The asymptotic analysis in Appendix A.2 shows that the CRLB approaches infinity in the unresolved region $\Delta kd \cos \theta < \gamma\pi$. It is also interesting to analyze how fast the CRLB approaches infinity to understand the ill-posedness of the inverse scattering problem. Here, we use numerical simulations that indicate that the CRLB basically grows exponentially with N , *i.e.*, $[\mathcal{I}_{\Gamma}^{-1}]_{nn} \sim \beta_n^N$. We consider reflection data with $B = 2$ that gives a FIM (3.9) with the sinc elements $f_n = \frac{\sin(2k_2 dn \cos \theta)}{2k_2 dn \cos \theta}$. The quotients between the CRLB of structures with $N+1$ and N slabs, *i.e.*,

$$\beta_n = \frac{[\mathcal{I}_{\Gamma}^{-1}(N+1)]_{nn}}{[\mathcal{I}_{\Gamma}^{-1}(N)]_{nn}} \quad (3.20)$$

are shown in Figure 3 for a multilayer structure with $N = 16, 18, 20, 22$ slabs. The results verify that it is necessary to have a very high signal-to-noise ratio to resolve

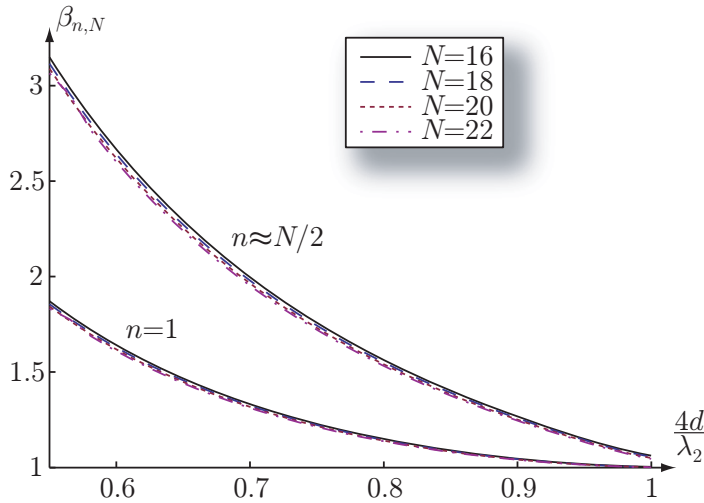


Figure 3: Illustration of the exponential growths of the CRLB. The estimated exponents $\beta_{n,N}$ by (3.20) in the region $d \leq \lambda_2/2$ for $B = 2$ and N slabs at for the edge, $n = 1$, and at the center, $n \approx N/2$.

structures with $d < \lambda_2/4$ even for moderately large N . Observe that $4d/\lambda_2 = 1$ corresponds to (3.12) and gives $\beta_{N/2} \approx 1 + 2/N \approx 1$ for large N .

Although, the FIM in (3.9) is based on a continuous range of frequencies it is sufficient to consider a set of discrete equidistant frequency samples $k_j = k_2 - \Delta k j/N_j$, $j = 0, 1, \dots, N_j - 1$ at the resolution limit $\Delta k d \cos \theta = \pi$. This gives the FIM in the form of a discrete Fourier transform

$$\begin{aligned}
 [\mathcal{I}_\Gamma]_{mn} &= \frac{2 \operatorname{Re}}{\sigma_\Gamma^2 N_j} \sum_{j=0}^{N_j-1} \frac{\partial \Gamma}{\partial \xi_m} \left(\frac{\partial \Gamma}{\partial \xi_n} \right)^* \\
 &= \frac{\operatorname{Re}}{2\tilde{\sigma}_\Gamma^2} \sum_{p=-1}^1 (-1)^p (1 + \delta_{p0}) e^{i2k_2 d(n-m-p) \cos \theta} \frac{1}{N_j} \sum_{j=0}^{N_j-1} e^{-i2\pi j(n-m-p)/N_j} \\
 &= \frac{1}{2\tilde{\sigma}_\Gamma^2} (2\delta_{n-m} - \delta_{n-m-1} - \delta_{n-m+1}), \quad (3.21)
 \end{aligned}$$

where the last equality holds for $n, m \leq N_j$. With $N_j = N$ we get the sampling $\Delta f/N = c_0 \Delta k / (2\pi N) = c_0 / (2dN \cos \theta)$. The corresponding time interval is $T = N/\Delta f = 2dN \cos \theta c_0^{-1}$. We can interpret the sampled case as a time-domain measurement with temporally periodic signals, *i.e.*, $E(t) = E(t + T)$. The requirement $T \geq N/\Delta f = 2dN \cos \theta c_0^{-1}$ is the time delay for the wave to propagate forward and back through the structure, *i.e.*, the two way traveling time [4, 15, 16]. The period time T decreases with increasing angle θ . Observe that this is in agreement with the results in [4].

4 FIM of the transmission coefficient

For observations of transmission data, we consider the FIM of the transmission coefficient evaluated at $\boldsymbol{\xi} = \mathbf{1}$. It is sufficient to analyze the transmission coefficient of an arbitrary single slab in the structure for this case. The transmission coefficient of slab number n is given by

$$\mathcal{T}_n = e^{-ik_{z,0}(L-d)} \frac{(1 - \rho_n^2)e^{-ik_{z,n}d}}{1 - \rho_n^2 e^{-2ik_{z,n}d}}, \quad (4.1)$$

with the derivative

$$\left. \frac{\partial \mathcal{T}_n}{\partial \xi} \right|_{\xi=1} = -id \frac{\partial k_z}{\partial \xi} e^{-ikL} = \frac{ikde^{-ikL}}{\cos \theta}. \quad (4.2)$$

This gives the FIM of the transmission coefficient at $\boldsymbol{\xi} = \mathbf{1}$ as

$$[\mathcal{I}_{\mathcal{T}}]_{mn} = \frac{2}{\sigma_{\mathcal{T}}^2 \Delta k} \operatorname{Re} \int_{k_1}^{k_2} \frac{k^2 d^2}{\cos^2 \theta} dk = \frac{(k_c d)^2}{2\sigma_{\mathcal{T}}^2 \cos^2 \theta} \left(4 + \frac{B^2}{12} \right) = \mathcal{I}_{\mathcal{T}}. \quad (4.3)$$

We observe that the FIM of transmission data is a rank 1 matrix with identical elements, *i.e.*, $\mathcal{I}_{\mathcal{T}} = \mathcal{I}_{\mathcal{T}} \mathbf{1} \mathbf{1}^T$, where $\mathbf{1}$ is the $N \times 1$ matrix with unit elements. Its non-zero subspace corresponds to the sum of all elements. This means that the transmission coefficient only contains information about the sum of all parameters. Obviously, the corresponding CRLB for estimating ξ_n is unbounded if $N > 1$. However, the transmission coefficient contains independent information from the reflection coefficient and can hence be used to improve the estimates of the parameters. The FIM of the combined observations of the reflection coefficient and the transmission coefficient is $\mathcal{I}_{\Gamma\mathcal{T}} = \mathcal{I}_{\Gamma} + \mathcal{I}_{\mathcal{T}} = \mathcal{I}_{\Gamma} + \mathcal{I}_{\mathcal{T}} \mathbf{1} \mathbf{1}^T$, where the inverse can be determined with the Sherman-Morrison formula [5]

$$\mathcal{I}_{\Gamma\mathcal{T}}^{-1} = \mathcal{I}_{\Gamma}^{-1} - \frac{\mathcal{I}_{\mathcal{T}}}{1 + \mathcal{I}_{\mathcal{T}} \mathbf{1}^T \mathcal{I}_{\Gamma}^{-1} \mathbf{1}} \mathcal{I}_{\Gamma}^{-1} \mathbf{1} \mathbf{1}^T \mathcal{I}_{\Gamma}^{-1} \quad (4.4)$$

with the explicit diagonal elements for $\Delta kd \cos \theta = \pi$ given by

$$[\mathcal{I}_{\Gamma\mathcal{T}}^{-1}]_{nn} = 2\tilde{\sigma}_{\Gamma}^2 \left(\frac{n(N+1-n)}{N+1} - \frac{\beta 3n^2(N-n+1)^2}{12 + \beta N(N+1)(N+2)} \right), \quad (4.5)$$

where $\beta = 2\tilde{\sigma}_{\Gamma}^2 \mathcal{I}_{\mathcal{T}}$, see Appendix A.1. The expression simplifies for large N , where we see that the CRLB of the slab in the center of the structure is approximately reduced a factor of 4. The diagonal elements are shown in Figure 4 for $N = 100, 200$ and $\beta = 10^{-p}$, $p = 1, 2, \dots, 6$ at the resolution limit $\Delta kd \cos \theta = \pi$.

5 Resolution versus accuracy

As the CRLB increases with the number of slabs in the structure, see (3.13) and Figure 4, it is possible to trade resolution with accuracy. Here, we consider a multi-layer structure with length $L = dN$. The CRLB for the slab in the center increases

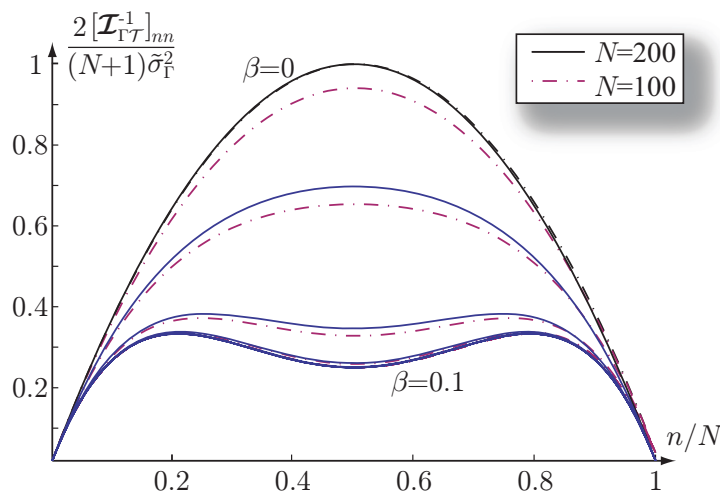


Figure 4: Cramér-Rao lower bound with reflection and transmission data as a function of the slab position, n , in the structure for the resolution $\Delta kd \cos \theta = \pi$, $N = 100, 200$, noise level $\tilde{\sigma}_{\Gamma}(N + 1) = 2$, and the quotient $\beta = 2\tilde{\sigma}_{\Gamma}^2 \mathcal{I}_{\mathcal{T}} = 10^{-p}$, for $p = 1, 2, \dots, 6$.

linearly in N for $\Delta kd \cos \theta = \pi$, *i.e.*, $\max_n [\mathcal{I}_{\Gamma}^{-1}]_{nn} = \tilde{\sigma}_{\Gamma}^2 (N + 1)/2$. This means that the accuracy increases with a reduced resolution. Use the shortest wavelength, λ_2 , to express the length, $L = N_{\lambda_2} \lambda_2$, and resolution, $d_{\lambda_2} = d/\lambda_2$. This gives the CRLB

$$\max_n [\mathcal{I}^{-1}]_{nn} \approx \tilde{\sigma}_{\Gamma}^2 \frac{N + 1}{2} = \tilde{\sigma}_{\Gamma}^2 \frac{N_{\lambda_2}/d_{\lambda_2} + 1}{2} \approx \tilde{\sigma}_{\Gamma}^2 \frac{N_{\lambda_2}}{2d_{\lambda_2}} \quad (5.1)$$

giving

$$\max_n [\mathcal{I}^{-1}]_{nn} d_{\lambda_2} \approx \frac{\tilde{\sigma}_{\Gamma}^2 N_{\lambda_2}}{2}. \quad (5.2)$$

Here, we observe that there is a trade off between resolution and accuracy in the form of an uncertainty relation, *i.e.*, we can trade increased resolution for reduced accuracy. It is important to emphasize that it is necessary that the resolution criteria (3.18) is fulfilled for the relation (5.2) to be valid. This also means that $d_{\lambda_2} \geq 1/4$.

The Cramér-Rao lower bound using reflection data is shown in Figure 5 for structures with lengths $L = m\lambda_2$, $m = 10, 50, 100$. The CRLB is determined with (3.9) and the fractional bandwidths $B = 1.5, 2$. It is observed that the CRLB oscillates around the approximate expression (5.2).

6 Lossy background

In many practical cases it is necessary to consider a lossy background. Here, we consider small losses in the form of a conductivity, *i.e.*,

$$kc_0 = (k_r + ik_i)c_0 = \omega \sqrt{\epsilon_{\infty} + \frac{\sigma}{i\omega}} \approx \epsilon_{\infty}^{1/2} \omega + \frac{\sigma}{2i\epsilon_{\infty}^{1/2}} \quad \text{if } \frac{\sigma}{\omega} \ll \epsilon_{\infty}. \quad (6.1)$$

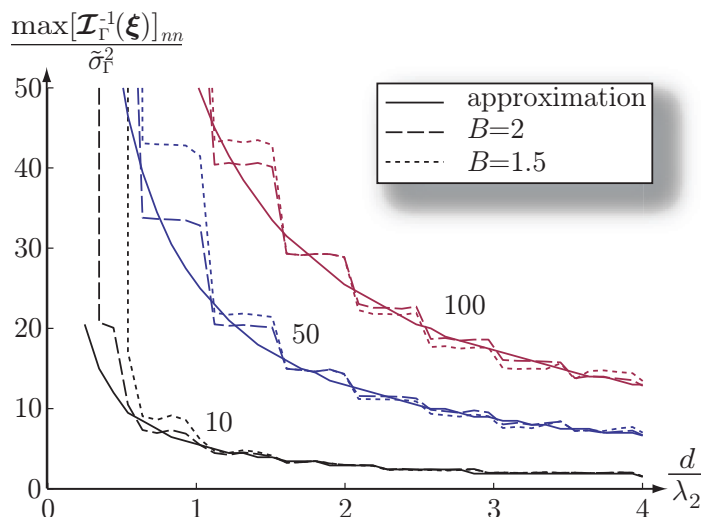


Figure 5: Cramér-Rao lower bound versus resolution for structures with lengths $L = m\lambda_2$, $m = 10, 50, 100$ given by reflection data (3.9) with $B = 1.5, 2$. The solid lines show the results of the approximate expression (5.2).

The derivative of the reflection coefficient (3.7) is generalized to

$$\left. \frac{\partial \Gamma_1}{\partial \xi_n} \right|_{\xi=1} = a^n e^{-2in_k d} \frac{1 - ae^{-2ik_r d}}{2} \quad (6.2)$$

where $a = e^{-2k_i d}$ and $\theta = 0$ are used to simplify the notation. The corresponding FIM is given by

$$\begin{aligned} [\mathcal{I}_\Gamma(\xi)]_{mn} &= \frac{1}{2\tilde{\sigma}^2 \Delta k} \operatorname{Re} \int_{k_1}^{k_2} 2e^{2ikd(n-m)} - e^{2ikd(n-m-1)} - e^{2ikd(n-m+1)} dk \\ &= \frac{1}{2\tilde{\sigma}^2} a^{m+n} ((1+a^2)f_{n-m} - af_{n-m-1} - af_{n-m+1}). \end{aligned} \quad (6.3)$$

It is illustrative to decompose the FIM into two separate effects. First, the reduced sensitivity of slabs far from the measurement surface due to the damping of the wave field, *i.e.*, $[\mathcal{I}]_{mm} > [\mathcal{I}]_{nn}$ if $m < n$ and $a < 1$. Secondly, the effect due to the correlations in ξ and the related resolution analysis in Section 3. The first effect due to the reduced sensitivity can easily be disguised by the simple parameter scaling

$$\bar{\xi}_n = a^n \xi_n. \quad (6.4)$$

This gives the FIM in $\bar{\xi}$ as the bidiagonal Toeplitz matrix

$$[\mathcal{I}_\Gamma(\bar{\xi})]_{mn} = \frac{1}{2\tilde{\sigma}^2} ((1+a^2)f_{n-m} - af_{n-m-1} - af_{n-m+1}). \quad (6.5)$$

Observe that this FIM is normalized such that the diagonal elements are identical, *i.e.*, the sensitivities of each individual parameter are identical. The basic properties

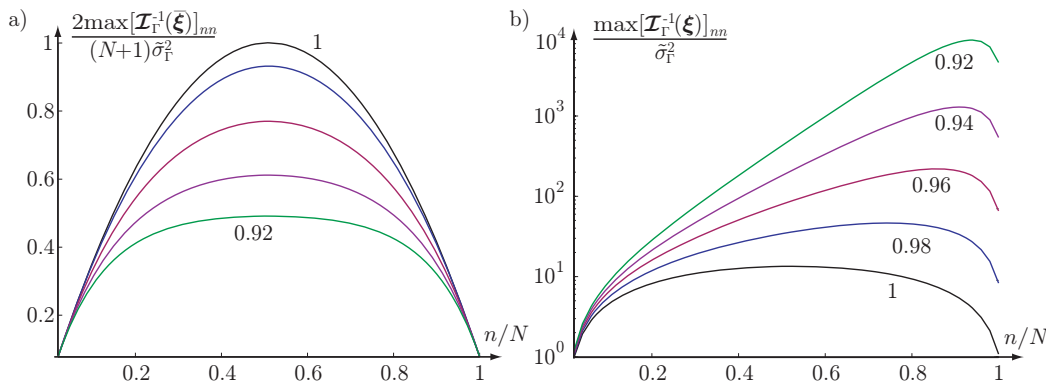


Figure 6: Cramér-Rao lower bound in a lossy structure with $N = 50$, $\Delta kd = \pi$, and $a = (1, 0.98, 0.96, 0.94, 0.92)$. a) for the scaled parameters $\bar{\xi}$. b) for the original parameters ξ .

of (6.5) are related to the bidiagonal Toeplitz matrix in (3.12) and summarized in Appendix A.1. The CRLB of $\bar{\xi}$ and ξ are related as

$$\text{var}\{\xi_n\} \geq [\mathcal{I}_\Gamma^{-1}(\xi)]_{nn} = a^{-2n} \text{var}\{\bar{\xi}_n\} \quad \text{where} \quad \text{var}\{\bar{\xi}_n\} \geq [\mathcal{I}_\Gamma^{-1}(\bar{\xi})]_{nn}. \quad (6.6)$$

The Cramér-Rao lower bound of the scaled, $\bar{\xi}$ and original, ξ , parameters are shown in Figure 6 for $a = (1, 0.98, 0.96, 0.94, 0.92)$, $N = 50$, and $\Delta kd = \pi$. It is seen that the CRLB of $\bar{\xi}$ reduces slightly whereas the CRLB of ξ increases fast as the loss increases. The decrease of $[\mathcal{I}^{-1}(\bar{\xi})]_{nn}$ shows that the effects of parameter correlations are reduced in the lossy background, *i.e.*, it is slightly easier to estimate a parameter in a lossy background than in a lossless background if the parameters have the same sensitivity $[\mathcal{I}]_{nn}$. However, as the wave decay exponentially in a lossy background the sensitivity of an object also decays exponentially.

7 Dispersive slabs

7.1 FIM of dispersive material parameters

Slabs are in general composed of several different materials with different electromagnetic properties, *e.g.*, an instantaneous response and a conductivity. In the general case of a dispersive slab, we can consider N_{ma} materials modeled as a sum of a general dispersion model of the form of several Debye and Lorentz terms [8, 11] where the permittivity in slab number n is

$$\epsilon_n(s) = \sum_{i=1}^{N_{\text{ma}}} \gamma_{ni} \langle \gamma_i \rangle \left\{ \epsilon_{\infty,i} + \frac{\sigma_i}{s} + \sum_{j=1}^{N_D} \frac{\beta_{D,ij}}{1 + \tau_{ij}s} + \sum_{j=1}^{N_L} \frac{\beta_{L,ij}}{1 + \nu_{ij}s + s^2 \omega_{0,ij}^{-2}} \right\} \quad (7.1)$$

where $s = i\omega$ and $\epsilon_{\infty,i}, \sigma_i, \beta_{D,ij}, \beta_{L,ij}$ are known material parameters. The inverse scattering problem consists of simultaneous estimation of the parameters γ_{ni} , $i =$

$1, 2, \dots, N_{\text{ma}}, n = 1, 2, \dots, N$ in the structure. Due to the frequency character of the parameters we scale the parameters with $\langle \gamma_i \rangle$ such that they obtain similar weights over the considered frequency range [8, 9]. The FIM of a multicomponent multilayer slab has the components

$$\begin{aligned} [\mathcal{I}_\Gamma(\gamma_i)]_{im,jn} &= \frac{2}{\sigma_\Gamma^2 \Delta\omega} \operatorname{Re} \int_{\omega_1}^{\omega_2} \left(\frac{\partial \Gamma}{\partial \xi_m} \frac{\partial \xi_m}{\partial \gamma_i} \right) \left(\frac{\partial \Gamma}{\partial \xi_n} \frac{\partial \xi_n}{\partial \gamma_j} \right)^* d\omega \\ &= \frac{2}{\sigma_\Gamma^2 \Delta\omega} \operatorname{Re} \int_{\omega_1}^{\omega_2} \frac{\partial \Gamma}{\partial \xi_m} \left(\frac{\partial \Gamma}{\partial \xi_n} \right)^* \frac{\partial \xi}{\partial \gamma_i} \left(\frac{\partial \xi}{\partial \gamma_j} \right)^* d\omega \\ &\approx \frac{2}{\sigma_\Gamma^2 \Delta\omega} \operatorname{Re} \frac{\partial \xi}{\partial \gamma_i} \left(\frac{\partial \xi}{\partial \gamma_j} \right)^* \int_{\omega_1}^{\omega_2} \frac{\partial \Gamma}{\partial \xi_m} \left(\frac{\partial \Gamma}{\partial \xi_n} \right)^* d\omega, \end{aligned} \quad (7.2)$$

where the last approximation is acceptable if the dispersion is negligible over the considered bandwidth. The simplified notation in (7.2) is justified as the differentials $\frac{\partial \xi_n}{\partial \gamma_{nj}}$ are independent of n . For the case where the dispersion is negligible we have a FIM in the form of a block matrix. Moreover, if the spatial part, $\mathcal{I}_\Gamma(\boldsymbol{\xi})$, is real valued, *e.g.*, at the resolution limit (3.11), we have

$$\mathcal{I}_\Gamma(\gamma_1, \gamma_2) \approx \mathcal{I}_\Gamma(\boldsymbol{\xi}) \otimes \begin{pmatrix} \alpha_{11} & \alpha_{12} \\ \alpha_{21} & \alpha_{22} \end{pmatrix} \quad (7.3)$$

for a two component composite, where $\alpha_{ij} = \operatorname{Re}\{\frac{\partial \xi}{\partial \gamma_i} \frac{\partial \xi}{\partial \gamma_j}\}$. The inverse is

$$\mathcal{I}_\Gamma^{-1}(\gamma_1, \gamma_2) \approx \frac{\mathcal{I}_\Gamma^{-1}(\boldsymbol{\xi})}{\alpha_{11}\alpha_{22} - \alpha_{12}\alpha_{21}} \otimes \begin{pmatrix} \alpha_{22} & -\alpha_{12} \\ -\alpha_{21} & \alpha_{11} \end{pmatrix}, \quad (7.4)$$

where \otimes denotes the Kronecker product [5].

The FIM together with the CRLB give fundamental limitations on the variance of any estimated parameter for every unbiased estimator. Even though the CRLB is invariant to scalings it is practical to normalize the parameters to simplify physical interpretations. This is especially important for parameters with different physical dimensions, *e.g.*, simultaneous estimation of the permittivity and the conductivity. This is also observed in gradient based optimization to inverse scattering [8, 9]. A normalization can also highlight the difference between the sensitivity of a single parameter and the ill-posedness due to combinations of the parameters.

The spatial and material parts of the FIM are coupled in the general case where the dispersion is not negligible. Although it is still important to normalize the parameters the normalization is not unique and it is not obvious how to choose a proper normalization [8, 9]. Here, we choose a scaling such that the sensitivity of each individual parameter is identical for small kd . The derivative of the reflection coefficient (3.7) is approximately

$$\left| \frac{\partial \Gamma}{\partial \xi_n} \right|_{\boldsymbol{\xi}=1}^2 = \frac{(1 - e^{-2ikd \cos \theta})^2}{4} (1 \pm \tan^2 \theta)^2 \sim k^2 d^2 \cos^2 \theta (1 \pm \tan^2 \theta)^2, \quad (7.5)$$

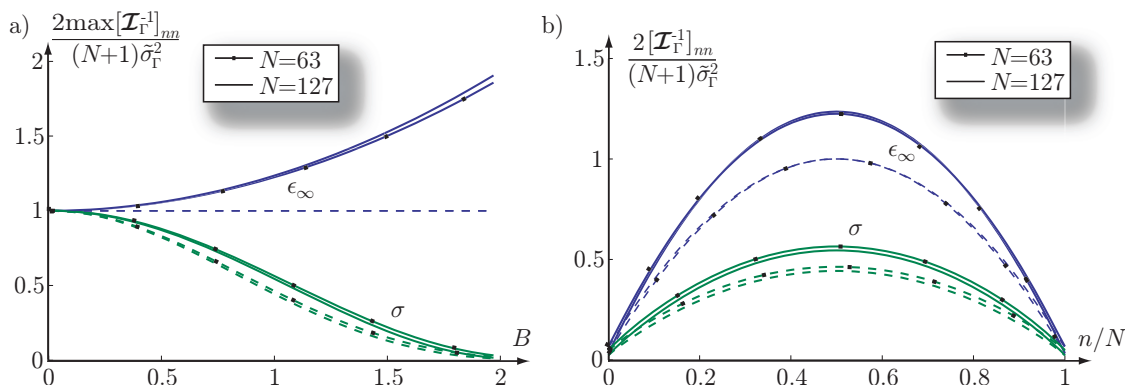


Figure 7: CRLB of the composite permittivity conductivity model (7.9) with $N = 63, 127$ slabs. a) comparison between the two parameter (solid lines) and single parameter (dashed lines) cases as a function of the relative bandwidth B for $n = (N + 1)/2$. b) CRLB for $B = 1$ as a function of the position.

where we observe that the frequency dependence is of the form ω^2 . This is the same dependence as for the transmission coefficient (4.3). The scaling parameters, $\langle \gamma_i \rangle$ are determined from the requirements

$$\frac{1}{\Delta\omega} \int_{\omega_1}^{\omega_2} \frac{\omega^2}{\omega_c^2} \left| \frac{\partial \xi}{\partial \gamma_i} \right|^2 d\omega = \frac{1}{\Delta\omega} \int_{\omega_1}^{\omega_2} \frac{\omega^2}{\omega_c^2} \left| \frac{\partial \xi}{\partial \gamma_j} \right|^2 d\omega \quad \text{for all } i, j. \quad (7.6)$$

The CRLB of the original parameters are obviously given by $\text{var}\{\gamma_i \langle \gamma_i \rangle\} = \langle \gamma_i \rangle^2 \text{var}\{\gamma_i\}$. Generalize the material coefficients in (7.3) to the dispersive case by defining the sensitivity parameters of the material parameters as the weighted projections

$$\alpha_{ij} = \frac{\text{Re}}{\Delta\omega} \int_{\omega_1}^{\omega_2} \frac{\omega^2}{\omega_c^2} \frac{\partial \xi}{\partial \gamma_i} \left(\frac{\partial \xi}{\partial \gamma_j} \right)^* d\omega. \quad (7.7)$$

Here, we consider a parameter normalization such that the sensitivity of each parameter is similar to simplify (7.4). Scale the parameters such that $\alpha_{11} = \alpha_{22} = 1$ and $\alpha = \alpha_{12} = \alpha_{21}$ to get

$$\mathcal{I}_{\Gamma}^{-1}(\gamma_1, \gamma_2) \approx \frac{\mathcal{I}_{\Gamma}^{-1}(\xi)}{1 - \alpha^2} \otimes \begin{pmatrix} 1 & -\alpha \\ -\alpha & 1 \end{pmatrix} \quad (7.8)$$

where we observe that the CRLB increases with $(1 - \alpha^2)^{-1}$. The approximation performed in (7.2), giving the block matrix in (7.8), is only valid if the dispersion is negligible over the considered bandwidth. The numerical examples in Section 7.3 verify that the approximation (7.8) together with (7.7) is accurate for narrow bandwidths.

7.2 Permittivity and conductivity

We consider simultaneous estimation of two material parameters. The material (7.1) is assumed to have a permittivity of the form of an instantaneous response and a

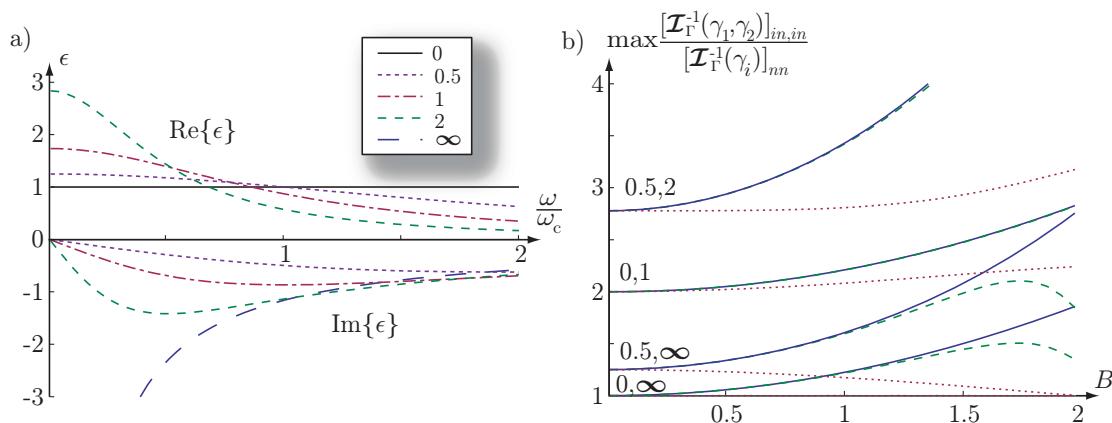


Figure 8: Estimation of the two component composite in a structure with 64 slabs. a) the frequency behavior of $\epsilon(\omega)$ for the generalized Debye models with $\tau = (0, 0.5, 1, 2, \infty)$. b) increase of the Cramér-Rao lower bound in the two composite Debye model from the single Debye case. The solid (dashed) line corresponds to the first (second) Debye parameter. The dotted line is the narrow band approximation (7.8).

conductivity, *i.e.*,

$$\epsilon_n(s) = \epsilon_{\infty,n} \langle \epsilon_{\infty} \rangle + \frac{\sigma_n \langle \sigma \rangle}{s} = \gamma_{n1} \langle \gamma_1 \rangle + \frac{\gamma_{n2} \langle \gamma_2 \rangle}{s}. \quad (7.9)$$

The scaling factors $\langle \gamma_i \rangle$ are given by the requirement that the sensitivities of the two parameter are approximately the same (7.6). The sensitivities with respect to ϵ_{∞} and σ are determined by the derivatives $\frac{\partial \epsilon}{\partial \epsilon_{\infty}} = \langle \epsilon_{\infty} \rangle$ and $\frac{\partial \epsilon}{\partial \sigma} = \frac{\langle \sigma \rangle}{i\omega}$ giving

$$\frac{1}{B\omega_0^3} \int_{\omega_1}^{\omega_2} \langle \epsilon_{\infty} \rangle^2 \omega^2 d\omega = \langle \epsilon_{\infty} \rangle^2 (1 + B/4) = \frac{1}{B\omega_0^3} \int_{\omega_1}^{\omega_2} \langle \sigma \rangle^2 d\omega = \frac{\langle \sigma \rangle^2}{\omega_c^2} \quad (7.10)$$

and hence $\langle \sigma \rangle = \langle \epsilon_{\infty} \rangle \omega_c \sqrt{1 + B/4}$.

The CRLB for the two parameters are shown in Figure 7a as a function of the relative bandwidth, B , for $\Delta kd \cos \theta = \pi$. In the figure, it is seen that the CRLB of the instantaneous response increases with B whereas the CRLB of the conductivity decreases with B . However, the effect of simultaneous estimation of both the permittivity and conductivity is not big and we can conclude that there is sufficient information in the reflection data to estimate the two parameters as long as the resolution condition (3.11) is fulfilled. The CRLB for the slabs as a function of the position are shown in Figure 7b for $B = 1$ and $N = 63, 127$. Here, we observe the similarities with the single parameter case depicted in Figure 4.

7.3 Debye models

A two composite Debye model is given by a permittivity of the form

$$\epsilon_{\tau_1, \tau_2}(s) = 1 + \frac{\gamma_1 \langle \gamma_1 \rangle}{1 + \tau_1 s} + \frac{\gamma_2 \langle \gamma_2 \rangle}{1 + \tau_2 s} \quad (7.11)$$

where the scaling factors $\langle \gamma_1 \rangle$ are determined by the condition (7.6). We observe that the special case of the instantaneous response and conductivity composite is given by the case $\epsilon_{0,\infty}$, *i.e.*, $\tau_1 = 0$ and $\tau_2 = \infty$. The real and imaginary parts of $\langle \gamma_j \rangle / (1 + i\omega\tau_j)$ are depicted in Figure 8a for the relative bandwidth $B = 2$ and $\tau_j = (0, 0.5, 1, 2, \infty)$. Observe that $\text{Im}\{\epsilon\} \leq 0$ for all passive materials and hence $\gamma_i(z) \geq 0$. Here, we do not use this additional information and hence consider the CRLB for estimating a general real valued $\gamma_i(z)$. This case is also motivated by the inverse scattering problem in a lossy background, see Section 6, where the signs of the parameters are unknown.

In Figure 8b, the increase of the CRLB in the two composite Debye case from the single Debye case for reflection data, *i.e.*,

$$\max_{1 \leq n \leq N} \frac{[\mathcal{I}_\Gamma^{-1}(\gamma_1, \gamma_2)]_{in,in}}{[\mathcal{I}_\Gamma^{-1}(\gamma_i)]_{nn}} \quad (7.12)$$

for $i = 1, 2$ are shown as a function of the relative bandwidth and various combinations of the Debye parameters. The CRLB is determined at the resolution limit $\Delta kd \cos \theta = \pi$, $N = 64$, and $k_{2,z}d = m\pi$ for any $m \geq 1$. The numerical simulations verify the narrow band approximation (7.8) as shown by the dotted lines.

8 Conclusions and discussion

The information content in reflection and transmission data of multilayer structures are analyzed. The Fisher information matrix together with the Cramér-Rao lower bound are used to give a strict definition of the information and to quantify the information in different measurement setups. It is shown that the reflection data contain more information than the transmission data in the low contrast limit. The resolution with reflection data is inversely proportional to the bandwidth and the Cramér-Rao lower bound increases linearly with the number of slabs. The Fisher information matrix of the transmission data is a rank one matrix that only contains information about the sum of the permittivities in the structure.

It is harder to estimate the parameters in a lossy background. It is shown that this is due to two separate effects: first the damping of the wave field that reduces the sensitivity of the parameters and secondly the effect of the correlation between parameters in the structure. Although, the exponential damping of the wave field dominates in a lossy background it is observed that the effect of the correlation is slightly reduced in a lossy background. Moreover, it is shown that the increased errors in the estimation of two dispersive material parameters in a multilayer structure can be understood by a weighted inner product related to the dispersive material models.

The Fisher information matrix and the Cramér-Rao lower bound used in this paper set a lower limit on what is possible but does not provide a constructive guidance in finding an algorithm that achieves this bound. Moreover, as the Cramér-Rao lower bound is a bound for unbiased estimators there might be biased estimators that perform better. It is also possible to use a priori information about the parameters, *i.e.*, physical limitations on the permittivity, as in Bayesian estimators to

improve the results [12]. However, the Cramér-Rao lower bound provides a good estimate on what is possible and what is not.

Although the Fisher information matrix is independent of the inversion algorithm there is a resemblance between the diagonal elements of the Fisher information matrix and the Fréchet differentials used in sensitivity analysis and least-squares approaches to inverse scattering. This can be partly understood by the relation between the Gaussian noise and the least-squares formulations [23]. The Fisher information matrix might also be useful for obtaining preconditioners for iterative approaches to inverse scattering in analogy with the parameter scaling derived from the diagonal elements in Section 7.

Acknowledgments

The financial support by the Swedish research council is gratefully acknowledged.

Appendix A Toeplitz matrices

In this appendix, we give the necessary details on the Toeplitz matrix (or convolution matrix) used in the analysis of the Fisher information matrix (3.9).

A.1 Bidiagonal matrix

The bidiagonal (or symmetric tridiagonal) matrix of the form

$$\mathbf{T}_1 = \begin{pmatrix} 2 & -1 & 0 & \dots & 0 \\ -1 & 2 & -1 & \dots & 0 \\ 0 & -1 & 2 & \dots & 0 \\ \vdots & \vdots & \vdots & \ddots & \vdots \\ 0 & 0 & 0 & \dots & 2 \end{pmatrix} \quad (\text{A.1})$$

has the inverse

$$\mathbf{T}_1^{-1} = \frac{1}{N+1} \begin{pmatrix} N & N-1 & N-2 & \dots & 1 \\ N-1 & 2(N-1) & 2(N-2) & \dots & 2 \\ N-2 & 2(N-2) & 3(N-2) & \dots & 3 \\ \vdots & \vdots & \vdots & \ddots & \vdots \\ 1 & 2 & 3 & \dots & N \end{pmatrix}, \quad (\text{A.2})$$

where we observe that the diagonal elements of the inverse are bounded as

$$\frac{N}{N+1} \leq [\mathbf{T}_1^{-1}]_{nn} = \frac{n(N+1-n)}{N+1} \leq \begin{cases} \frac{N+1}{4} & N \text{ odd} \\ \frac{N(N+2)}{4(N+1)} & N \text{ even} \end{cases} \quad (\text{A.3})$$

We also consider the inverse of $\mathbf{T}_1 + \beta \mathbf{1}\mathbf{1}^T$ where $\mathbf{1}$ is the $N \times 1$ matrix with unit elements. Use the Sherman-Morrison formula [5] to get

$$(\mathbf{T}_1 + \beta \mathbf{1}\mathbf{1}^T)^{-1} = \mathbf{T}_1^{-1} - \frac{\beta}{1 + \beta \mathbf{b}^T \mathbf{1}} \mathbf{b}\mathbf{b}^T \quad (\text{A.4})$$

where $\mathbf{b} = \mathbf{T}_1^{-1} \mathbf{1}$, *i.e.*, $[\mathbf{b}]_n = n(N - n + 1)/2$. Hence, we have the diagonal elements

$$\begin{aligned} [(\mathbf{T}_1 + \beta \mathbf{1}\mathbf{1}^T)^{-1}]_{nn} &= \frac{n(N + 1 - n)}{N + 1} - \frac{\beta 3n^2(N - n + 1)^2}{12 + \beta N(N + 1)(N + 2)} \\ &\approx \frac{n(N + 1 - n)}{N + 1} \left(1 - \frac{3n(N - n + 1)}{N(N + 2)} \right) \end{aligned} \quad (\text{A.5})$$

and for $n = (N + 1)/2$ we have

$$\frac{(N + 1)(N^2 + 2N - 3)}{16N(N + 2)} \approx \frac{N}{16}. \quad (\text{A.6})$$

The assumption of a weakly lossy medium (6.1), gives a corresponding bidiagonal Toeplitz matrix of the form

$$\mathbf{T}_\alpha = \begin{pmatrix} 1 + \alpha^2 & -\alpha & 0 & \dots & 0 \\ -\alpha & 1 + \alpha^2 & -\alpha & \dots & 0 \\ 0 & -\alpha & 1 + \alpha^2 & \dots & 0 \\ \vdots & \vdots & \vdots & \ddots & \vdots \\ 0 & 0 & 0 & \dots & 1 + \alpha^2 \end{pmatrix} = \alpha \mathbf{T}_1 + (1 - \alpha)^2 \mathbf{I}. \quad (\text{A.7})$$

The diagonal elements of the inverse of the matrix are

$$[\mathbf{T}_\alpha^{-1}]_{nn} = \alpha^{-n} \frac{(1 - \alpha^{2n})(1 - \alpha^{2(N+1-n)})}{(1 - \alpha^2)(1 - \alpha^{2(N+1)})} \quad (\text{A.8})$$

and specially for $n = (N + 1)/2$

$$[\mathbf{T}_\alpha^{-1}]_{nn} = \frac{1 - \alpha^{N+1}}{(1 - \alpha^2)(1 + \alpha^{N+1})}. \quad (\text{A.9})$$

A.2 Asymptotic behavior

Some basic properties of the Toeplitz matrix $[\mathbf{T}_N]_{ij} = f_{i-j}$, $i, j = 0, 1, \dots, N - 1$ can be analyzed with Fourier analysis in the asymptotic limit of an infinite matrix, *i.e.*, $N \rightarrow \infty$, *cf.*, the fundamental eigenvalue distribution theorem by Szegö [6, 7]. Here, we employ the Fourier series expansion of the matrix elements f_n given by

$$\hat{f}(\kappa) = \sum_{n=-\infty}^{\infty} f_n e^{in\pi\kappa} \quad (\text{A.10})$$

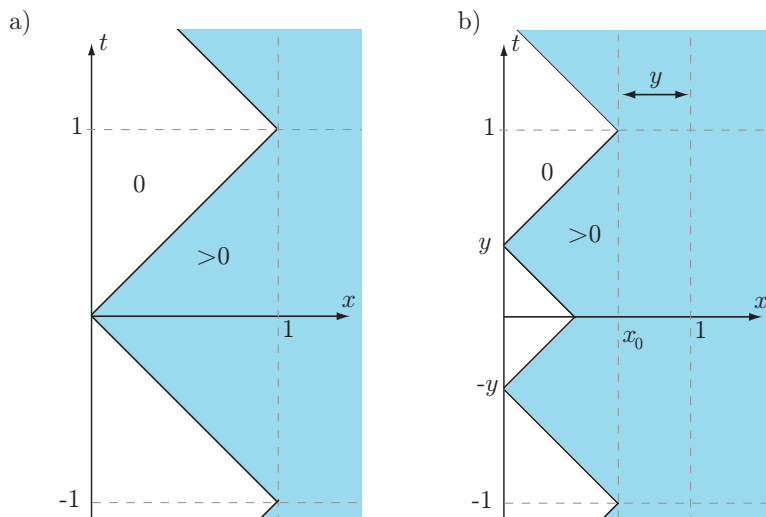


Figure 9: a) the stability region of the infinite dimensional sinc-Toeplitz matrix. b) the stability region of the infinite dimensional sinc-Toeplitz matrix.

which is a 2 periodic function in κ , *i.e.*, $\hat{f}(\kappa + 2) = \hat{f}(\kappa)$. Note that $\hat{f}(\kappa)$ is even for symmetric Toeplitz matrices, $f_n = f_{-n}$, and real valued for Hermitian matrices, $f_n = f_{-n}^*$. The function $\hat{f}(\kappa)$ can be used to establish bounds on the eigenvalues, $\lambda_{N,k}$, of finite dimensional Hermitian Toeplitz matrices as

$$\operatorname{ess\,inf}_{\kappa \in \mathbb{R}} \hat{f}(\kappa) \leq \lambda_{N,k} \leq \operatorname{ess\,sup}_{\kappa \in \mathbb{R}} \hat{f}(\kappa). \quad (\text{A.11})$$

Furthermore, under suitable assumptions the theorem by Szegő can be applied to show that

$$\lim_{N \rightarrow \infty} \frac{1}{N} \log \det \mathbf{T}_N = \frac{1}{2} \int_{-1}^1 \log \hat{f}(\kappa) \, d\kappa \quad (\text{A.12})$$

describing the limiting behavior of Toeplitz determinants. Obviously, a necessary condition for the infinite Toeplitz matrix to be invertible is that $\hat{f}(\kappa) > 0$ for all κ , except for at most a discrete set of points in $[-1, 1]$. Thus, if $\hat{f}(\kappa) = 0$ on an interval, the infinite Toeplitz matrix is singular.

The FIM (3.9) is a symmetric Toeplitz matrix with elements

$$[\mathbf{F}(x, y)]_{mn} = 2f_{m-n}(x, y) - f_{m-n-1}(x, y) - f_{m-n+1}(x, y) \quad (\text{A.13})$$

where

$$f_n(x, y) = \cos(n\pi y) \frac{\sin(n\pi x)}{n\pi x}. \quad (\text{A.14})$$

The Fourier series expansion of the three terms gives

$$\hat{F}(x, y, \kappa) = \sum_{n=-\infty}^{\infty} (2f_n - f_{n-1} - f_{n+1}) e^{in\pi\kappa} = 2(1 - \cos(\pi\kappa)) \hat{f}(x, y, \kappa) \quad (\text{A.15})$$

where

$$\hat{f}(x, y, \kappa) = \sum_{n=-\infty}^{\infty} f_n(x, y) e^{in\pi\kappa} = \frac{1}{2} \hat{g}(x, \kappa - y) + \frac{1}{2} \hat{g}(x, \kappa + y) \quad (\text{A.16})$$

and $\hat{g}(x, \kappa)$ is the Fourier series expansion of the sinc-term

$$\hat{g}(x, \kappa) = \sum_{n=-\infty}^{\infty} \frac{\sin(n\pi x)}{n\pi x} e^{in\pi\kappa}. \quad (\text{A.17})$$

Note that the variable x takes the role of a sampling interval for the continuous sinc-function $\frac{\sin(\pi\tau)}{\pi\tau}$ with $\tau = nx$. By using the sampling theorem and the Poisson summation formula [19] it is readily established that

$$\hat{g}(x, \kappa) = \begin{cases} 2\delta(\kappa) & x = 0 \\ 0 & 0 < x < |\kappa| \leq 1 \\ \frac{1}{x} & 0 < |\kappa| \leq x < 1 \\ 1 & x = 1, 2, 3, \dots \\ \frac{2m+\chi\hat{g}(x,\kappa)}{2m+\chi} > 0 & |x| > 1 \end{cases} \quad (\text{A.18})$$

where the last line corresponds to the aliasing case with $x = 2m + \chi$, $m = 1, 2, \dots$ and $0 < |\chi| < 1$. Note that the limit for aliasing is given by $x = 1$. In the present analysis it is sufficient to use that $\hat{g}(x, \kappa) = \hat{g}(x, \kappa + 2)$ and $\hat{g}(x, \kappa) > 0$ if $x > |\kappa|$ for $|\kappa| < 1$, see also Figure 9 where this region is illustrated. Finally, we obtain the Fourier series expansion in (A.15) as

$$\hat{F}(x, y, \kappa) = (1 - \cos(\pi\kappa))(\hat{g}(x, \kappa - y) + \hat{g}(x, \kappa + y)) \quad (\text{A.19})$$

where $\hat{g}(x, \kappa)$ is given by (A.18).

As we analyze the properties of the inverse of \mathbf{F} , we need to investigate the conditions on x, y such that $\hat{F}(x, y, \kappa) > 0$ for all κ . We observe that it is necessary that $(1 - \cos(\pi\kappa)) > 0$ and that either $\hat{g}(x, \kappa - y) > 0$ or $\hat{g}(x, \kappa + y) > 0$ for all κ . The first term $(1 - \cos(\pi\kappa))$ is positive for all κ except for $\kappa = 0$. This indicates that it may not be possible to invert the Toeplitz matrix in the limit $N \rightarrow \infty$. However, the point $\kappa = 0$ only gives rise to a linear growth in N of the inverse and is hence not a major problem if N is not too large. For the second and more important requirement that $\hat{g}(x, \kappa + y) + \hat{g}(x, \kappa - y) > 0$ for all κ we use Figure 9 where the region for $\hat{g}(x, \kappa) > 0$ and $\hat{g}(x, \kappa \pm y) > 0$ are depicted. We observe that the region for $\hat{g}(x, \kappa \pm y) > 0$ increases for $0 < y < 1/2$ to reach its maximal size for $y = 1/2$ and then decreases for $1/2 < y < 1$. Obviously, the maximal region given by $y = 1/2 + m$, $m \in \mathbb{Z}$ corresponds to $x > x_0 = 1/2$. For general shifts y , we have a maximal region given by

$$x > x_0 = 1 - \min_{m \in \mathbb{Z}} (|y - m|) = \frac{1}{2} + \min_{m \in \mathbb{Z}} (|y - \frac{1}{2} - m|). \quad (\text{A.20})$$

Finally, we illustrate the ill-conditioning of the $N \times N$ Toeplitz matrix $[\mathbf{F}(x, y)]_{mn}$ for $x < 1$ and $y = 0$ using

$$[\mathbf{F}(x, 0)]_{mn} = 2f_{m-n}(x, 0) - f_{m-n-1}(x, 0) - f_{m-n+1}(x, 0) \quad (\text{A.21})$$

where

$$f_n(x, 0) = \frac{\sin(n\pi x)}{n\pi x}. \quad (\text{A.22})$$

The largest value of the diagonal elements divided with $(N+1)/4$, *i.e.*, $4[\mathbf{F}^{-1}(x)]_{nn}/(N+1)$, are plotted in Figure 10 for $0.8 \leq x \leq 1.1$ and $N = 25, 50, 100, 200$.

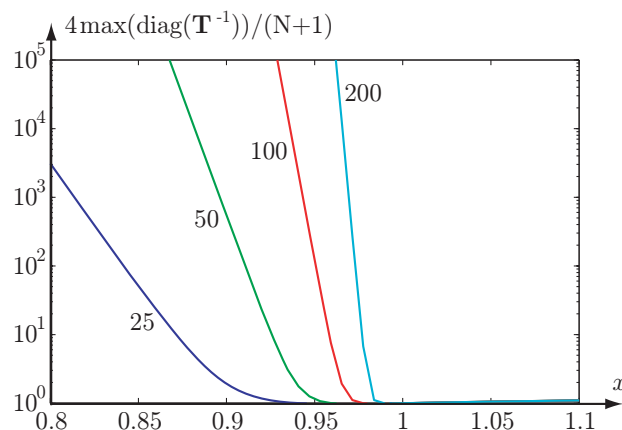


Figure 10: Dependence of the inverse of the sinc-Toeplitz matrix on the matrix size, *i.e.*, $\max_n 4[\mathbf{G}^{-1}(x)]_{nn}/(N+1)$ for $N = 25, 50, 100, 200$.

References

- [1] M. Bertero. Linear inverse and ill-posed problems. *Advances in electronics and electron physics*, **75**, 1–120, 1989.
- [2] K. Bube and R. J. Burridge. The one-dimensional inverse problem of reflection seismology. *SIAM Review*, **25**(4), 497–559, 1983.
- [3] O. M. Bucci, L. Crocco, T. Isernia, and V. Pascazio. Subsurface inverse scattering problems: Quantifying qualifying and achieving the available information. *IEEE Trans. Geoscience and Remote Sensing*, **39**(11), 2527–2538, November 2001.
- [4] J. P. Coronés and A. Karlsson. Transient direct and inverse scattering for inhomogeneous viscoelastic media: obliquely incident SH mode. *Inverse Problems*, **4**, 643–660, 1988.
- [5] G. H. Golub and C. F. van Loan. *Matrix Computations*. The Johns Hopkins University Press, Baltimore, Maryland, 1983.
- [6] R. M. Gray. On the asymptotic eigenvalue distribution of Toeplitz matrices. *IEEE Trans. Information Theory*, **18**, 725–730, November 1972.
- [7] U. Grenander and G. Szegő. *Toeplitz forms and their applications*. University of California Press, Berkeley, Los Angeles, 1958.
- [8] M. Gustafsson. *Wave Splitting in Direct and Inverse Scattering Problems*. PhD thesis, Lund Institute of Technology, Department of Electromagnetic Theory, P.O. Box 118, S-221 00 Lund, Sweden, 2000. <http://www.es.lth.se/home/mats>.
- [9] M. Gustafsson and S. He. An optimization approach to two-dimensional time domain electromagnetic inverse problems. *Radio Sci.*, **35**(2), 525–536, 2000.

- [10] V. Isakov. *Inverse Problems for Partial Differential Equations*. Springer-Verlag, Berlin, 1998.
- [11] J. D. Jackson. *Classical Electrodynamics*. John Wiley & Sons, New York, third edition, 1999.
- [12] S. M. Kay. *Fundamentals of Statistical Signal Processing, Estimation Theory*. Prentice-Hall, Inc., NJ, 1993.
- [13] A. Kirsch. *An Introduction to the Mathematical Theory of Inverse Problems*. Springer-Verlag, New York, 1996.
- [14] H. Krim and M. Viberg. Two decades of array signal processing research: the parametric approach. *IEEE Signal Processing Magazine*, **13**(4), 67–94, July 1996.
- [15] G. Kristensson and R. J. Krueger. Direct and inverse scattering in the time domain for a dissipative wave equation. Part 1: Scattering operators. *J. Math. Phys.*, **27**(6), 1667–1682, 1986.
- [16] G. Kristensson and R. J. Krueger. Direct and inverse scattering in the time domain for a dissipative wave equation. Part 2: Simultaneous reconstruction of dissipation and phase velocity profiles. *J. Math. Phys.*, **27**(6), 1683–1693, 1986.
- [17] S. Nordebo, M. Gustafsson, and K. Persson. Sensitivity analysis for antenna near-field imaging. Technical Report LUTEDX/(TEAT-7139)/1–17/(2005), Lund Institute of Technology, Department of Electrosience, P.O. Box 118, S-211 00 Lund, Sweden, 2005. www.es.lth.se/teore1/.
- [18] S. Nordebo and M. Gustafsson. Statistical signal analysis for the inverse source problem of electromagnetics. Technical Report LUTEDX/(TEAT-7136)/1–12/(2005), Lund Institute of Technology, Department of Electrosience, P.O. Box 118, S-211 00 Lund, Sweden, 2005. <http://www.es.lth.se/teore1>, Accepted by IEEE Trans. Signal Process.
- [19] A. V. Oppenheim and R. W. Schaffer. *Digital Signal Processing*. Prentice-Hall, Inc., Englewood Cliffs, New Jersey, 1975.
- [20] S. J. Orfanidis. Electromagnetic waves and antennas, 2002. www.ece.rutgers.edu/~orfanidi/ewa, revision date June 21, 2004.
- [21] R. Pierri and F. Soldovieri. On the information content of the radiated fields in the near zone over bounded domains. *Inverse Problems*, **14**(2), 321–337, 1998.
- [22] T. Söderström and P. Stoica. *System Identification*. Prentice Hall, 2001.
- [23] A. Tarantola. *Inverse Problem Theory*. SIAM, Philadelphia, 2005.
- [24] A. G. Tijhuis. *Electromagnetic Inverse Profiling. Theory and Numerical Implementation*. VNU Science Press BV, Utrecht, 1987.